Dalton Transactions

PAPER

View Article Online
View Journal | View Issue

Cite this: *Dalton Trans.*, 2016, **45**, 539

Pd–$Co_3[Co(CN)_6]_2$ hybrid nanoparticles: preparation, characterization, and challenge for the Suzuki–Miyaura coupling of aryl chlorides under mild conditions†

Ren Li,*[a,c] Ran Li,[a] Changlai Wang,[a] Lei Gao[b] and Qianwang Chen*[a,b]

Received 16th September 2015,
Accepted 6th November 2015

DOI: 10.1039/c5dt03631c

www.rsc.org/dalton

Because of their abundance and low cost, organo chlorides are the most desirable substrates from the industrial point of view in Suzuki–Miyaura cross-coupling reactions. However, catalytic application of Pd nanoparticles (NPs) for Suzuki coupling of aryl chlorides is still a challenge. Here, we design a novel catalyst by combining Pd NPs with $Co_3[Co(CN)_6]_2$ nanocrystals for Suzuki–Miyaura coupling of aryl chlorides. This nanocatalyst demonstrated good activity (yield 86.2% at 80 °C), high TOF, great stability, easy separation, excellent reusability (initial rates were not reduced after five cycles) and low cost in Suzuki reactions.

Introduction

Suzuki–Miyaura cross-coupling reactions, among the most widely used protocols for the formation of carbon–carbon bonds, have become one of the most efficient synthetic methods for the synthesis of biaryl compounds, which include a wide range of natural products and pharmaceuticals.[1] These reactions are generally catalyzed by soluble palladium (Pd) complexes or Pd NPs with various ligands in organic solvents and, more recently, in aqueous media as well.[2] Activation of the Pd pre-catalyst is followed by oxidative addition of the halogenated (X = Cl, Br, I) substrates. Coupling reactions of these substrates typically decrease in difficulty in the order of R–Cl > R–Br > R–I. This can be explained in terms of the R–X bond dissociation enthalpies (BDE). For example, the X–Ph BDE range from X–Cl = 95.5 ± 1.5 kcal mol^{-1}; X–Br = 80.4 ± 1.5 kcal mol^{-1} to X–I = 65.0 ± 1 kcal mol^{-1}.[3] Due to their abundance and low cost, organo chlorides are the most desirable substrates from the industrial point of view.[4] In traditional protocols, the Pd chelate catalysts with organo phosphine ligands, such as triphenylphosphine (PPh_3),[5] N-heterocyclic carbenes (NHC)[6] and palladacycle complexes[7] have been established for the Suzuki coupling of aryl chlorides. However, these chelates sometimes require multistep syntheses and/or rigorously anhydrous and inert conditions even if the intermediate carbene ligand is not isolated.[8] Additionally, the high air-sensitivity of the complex makes the catalyst recovery/recycling difficult, and thus an excess amount of chelates is usually required to achieve a reasonable catalytic activity.[9] In particular, these homogeneous catalysts are difficult to be separated, recovered and reused. Pd NPs, which enjoy several advantages such as excellent activity, greater selectivity, and high stability over conventional catalyst systems, partially due to their large surface-to-volume ratios, are widely used for C–C cross coupling reactions.[10] But, Pd NPs were not used as appropriate catalysts for aryl chloride transformation due to the low yield and high temperature conditions (mostly up to 100 °C) and long reaction times. Therefore, developing a new type of nanocatalyst having both the advantages of homogeneous (*e.g.*, high selectivity, high turn-over numbers, and effortless optimization of reaction activity) and heterogeneous catalysis (*e.g.*, easy separation, recovery and low cost) is still a goal of nanocatalyst design.

Porous materials with large surface area have attracted significant scientific attention because of their diverse potential applications in separation,[11] gas storage,[12] and especially heterogeneous catalysis.[13] In the last few decades, the surge to develop such useful materials has led scientists to prepare a number of novel porous materials such as metal organic frameworks (MOFs),[14] porous organic cages,[15] and microporous organic polymers (MOPs)[16] in addition to traditional porous materials such as zeolites and activated carbon. Among these porous materials, MOFs have attracted particular attention due to their unique properties such as large surface area, low skeletal density, and high chemical stability.[17] The use of MOFs as solid catalysts is significantly interesting due to their

[a]*Hefei National Laboratory for Physical Science at Microscales, Department of Materials Science & Engineering, Collaborative Innovation Center of Suzhou Nano Science and Technology, University of Science and Technology of China, Hefei, China. E-mail: liren@ustc.edu.cn, cqw@ustc.edu.cn*
[b]*High Magnetic Field Laboratory, Chinese Academy of Sciences, Hefei, China*
[c]*Laboratory of Inorganic Materials Chemistry (CMI), University of Namur, 61 rue de Bruxelles, B-5000 Namur, Belgium*
†Electronic supplementary information (ESI) available. See DOI: 10.1039/c5dt03631c

large pore sizes being favorable for the diffusion of large substrates and products.[18] Furthermore, it is often possible to tailor the pore structure and functionality to yield the chemo-, regio-, stereo- and/or enantioselectivity by creating an appropriate environment around the catalytic center in the restricted space available.[19] Moreover, it is possible to have a homogeneous distribution of one or more active sites due to their high degree of crystallinity.[20] MOFs can also be used as host matrices to support the catalysts, as in the case of mesoporous silicates.[21] Much effort has focused on the encapsulation of metal NPs inside the cavities of MOFs (metals@MOFs), which can be synthesized by solution- or gas-phase loading methods, which depend on the different metal precursors. In particular, the incipient wetness impregnation is a largely used method for this fabrication, because common inorganic salts are adoptable as precursors.[21] The mechanically robust walls of the frameworks can be utilized to confine metal NPs and restrict their growth.[22] The good dispersivity of NPs within the frameworks makes them more accessible to reactants, thereby exhibiting excellent catalytic activity.[22] Additionally, a variety of structural features can engender catalytic activity in MOFs, such as open metal sites at framework nodes, which often have unique coordination environments, and metal or organic centered catalytic units that are integrated, as well as active metal NPs that are grown and stabilized within the cavities.[23] Moreover, a combination of active metal NPs with the functionalities within the host, multifunctional catalysts capable of promoting different reactions or one-pot cascade reactions can thus be realized.[24] The Pd@MOFs were firstly tested for C–C coupling reactions in 2008, and Hwang and Férey *et al.*[25] demonstrated that Pd@ED-grafted-MIL-101(Cr) and Pd@APS-grafted-MIL-101(Cr), which were obtained by anionic exchange reactions followed by $NaBH_4$ reduction, had obviously high activities during the Heck reaction of acrylic acid with iodobenzene, and their activities were comparable with that of a commercial Pd/C catalyst (1.09 wt% Pd) after a certain induction period (0.5–1 h). The good recyclability of Pd-loaded MIL-101(Cr) verified the heterogeneous catalytic nature.

Prussian blue analogues (PBA) have been paid growing attention for their applications in hydrogen molecular magnetics,[26] storage,[27] optics,[28] and so on.[29] However, employing PBA as the catalyst or catalyst supports in liquid reactions has not been reported. According to our previous work,[30,31] nanosized $Co_3[Co(CN)_6]_2$, which can serve as efficient adsorbents for adsorbing heavy metal ions[32] and organic dyes[33] from aqueous solutions, with ultrahigh specific surface area and abundant micropores was achieved at room temperature *via* a one-step process. Herein, we demonstrate the construction of easily separable and high activity Pd nanocatalysts through deposition of Pd NPs on the surface of PBA nanocrystals. To evaluate the activity and stability of the supported Pd nanocatalysts, Suzuki coupling reactions were chosen as the model reaction for the test. The results indicate that this catalyst not only shows outstanding activity especially for aryl chloride reactions, but can also be easily separated from the reaction medium and reused for several cycles without an obvious decrease of conversion rate.

Results and discussion

The crystallinity and phase composition of the resulting products were investigated by X-ray powder diffraction (XRD). Fig. 1 shows the XRD patterns of the samples. Compared with the XRD patterns of the pure MOF nanoclusters reported previously, new reflection peaks which corresponded to the 111 and 220 of face-centered cubic Pd nanocrystals were observed. According to the Debye–Scherrer equation, the diameter of Pd NPs is calculated to be 3 nm, which is well in agreement with that observed from TEM.

The morphology of the hybrid NPs shows a core–shell like feature with fine Pd particles deposited on the $Co_3[Co(CN)_6]_2$ surface, as shown in Fig. 2a. It is easily observed that the diameter of the as-prepared MOF NPs is about 100 nm in size. It can also be found that the surface of $Co_3[Co(CN)_6]_2$ NPs are decorated with several nanometers diameter NPs. The high-resolution TEM image of a single core shell hybrid nanoparticle from Fig. 2b suggests that the palladium NPs are

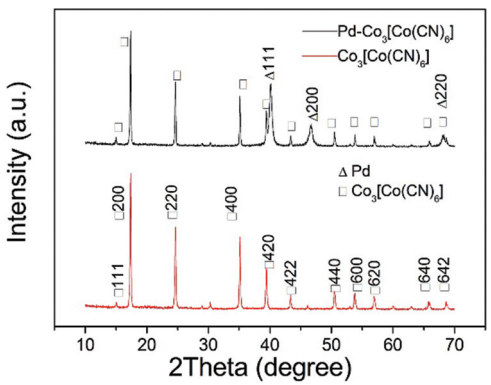

Fig. 1 XRD pattern of Pd–$Co_3[Co(CN)_6]_2$ hybrid NPs and $Co_3[Co(CN)_6]_2$ NPs.

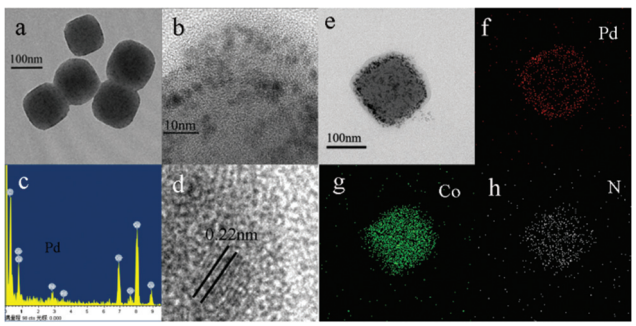

Fig. 2 Characterization of Pd–$Co_3[Co(CN)_6]_2$ hybrid NPs: (a) TEM image; (b) HRTEM image of a $Co_3[Co(CN)_6]_2$ hybrid nanoparticle; (c) EDAX of a Pd nanoparticle; (d) lattice fringe and electron diffraction (ED) of a single Pd nanoparticle. (e) HAADFS-TEM image of a single nanostructure. (f) Elemental map of Pd on the nanostructure shown in (e). (g) Corresponding elemental map of Co. (h) Corresponding elemental map of N.

encapsulated within the micropores; it is easy to find that the particle size was about 3 nm. Energy dispersive analysis of X-rays (Fig. 2c) of the selected areas further reveals their elemental composition, including Pd, Co, C, N and Cu. The Pd signal shows that the palladium chloride has been successfully reduced and deposited on the surface of MOF nanoclusters. The clear 2D lattice fringes of Pd nanocrystals are shown in Fig. 2d. The inter planar distance is about 0.2 nm, which corresponds well to the (111) lattice plane of Pd. Elemental mapping of Co, N and Pd (Fig. 2e–2h) also revealed that the nanostructures were composed of different segments. In particular, the as-prepared Pd–MOF nanocrystals are essentially cube-like nano structures in which Pd encircles a pure $Co_3[Co(CN)_6]_2$ core.

Fig. 3 exhibits the FT-IR spectra of Pd–$Co_3[Co(CN)_6]_2$ and $Co_3[Co(CN)_6]_2$ NPs synthesized in this work. In the spectrum, the characteristic peaks at round 2170 cm^{-1} are assigned to C≡N bond stretching. The presence of crystal water can be deduced from the occurrence of a sharp n(O–H) band due to the water incorporated in the crystalline lattice (3645 cm^{-1}) and from the occurrence of the $d(OH_2)$ vibration (1610 cm^{-1}). There is not too much difference between Pd–$Co_3[Co(CN)_6]_2$ and $Co_3[Co(CN)_6]_2$ spectra, which indicated that there is no obvious group change in the Pd–$Co_3[Co(CN)_6]_2$ prepared section.

XPS spectroscopy, one of the most important techniques to determine the oxidation state of the surface element in materials, was used to characterize the Pd–$Co_3[Co(CN)_6]_2$ composites. The inset figure of Fig. 4 shows the survey spectrum of the Pd–$Co_3[Co(CN)_6]_2$ composites. The signal of the Pd element is nearly the same as that of the Co element, which implies that $Co_3[Co(CN)_6]_2$ is almost fully covered by Pd NPs. This phenomenon is well in agreement with what has been observed in the TEM. The XPS spectrum of Pd 3d can be fitted into two main doublet peaks, as shown in Fig. 4. The binding energy of the doublet peaks at 335.4 eV (assigned to Pd^0 $3d_{5/2}$) and 340.7 eV (assigned to Pd^0 $3d_{3/2}$) can be attributed to the Pd(0) state. The above results indicate that Pd species on the surface of $Co_3[Co(CN)_6]_2$ nanospheres was elementary Pd(0).

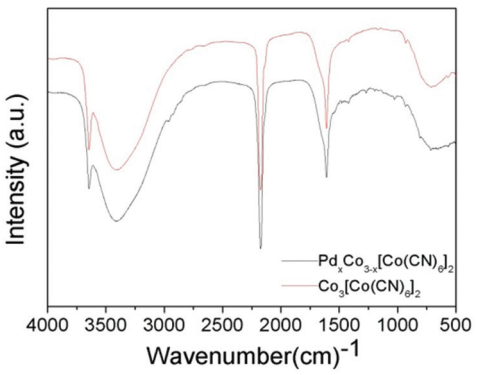

Fig. 3 FT-IR spectra of $Co_3[Co(CN)_6]_2$ NPs and Pd–$Co_3[Co(CN)_6]_2$ hybrid NPs.

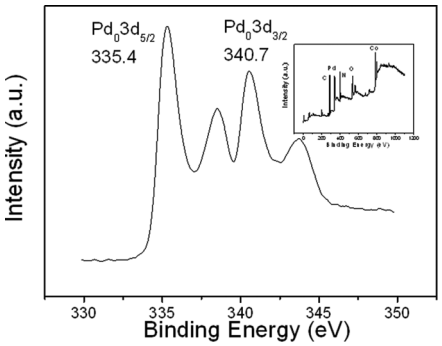

Fig. 4 XPS of the Pd 3d spectrum in Pd–$Co_3[Co(CN)_6]_2$, the inset is the survey XPS spectrum of Pd–$Co_3[Co(CN)_6]_2$ hybrid NPs.

The other two peaks are related to Pd(II) species, which may be due to some Pd^{2+} doping into $Co_3[Co(CN)_6]_2$. In particular, the value of binding energy is similar to $K_2Pd_2(CN)_4$, whose Pd^0 $3d_{5/2}$ state equals 338.8 eV and Pd^{II} $3d_{3/2}$ state equals 334 eV, indicating that Pd combined with C≡N.[34] The above results indicate that some Pd atoms were doped into the lattice of $Co_3[Co(CN)_6]_2$ nanocubes. To ensure Pd^{2+} was not adsorbed but doped, the nanocatalyst was washed with deionized water several times and then dissolved in nitromuriatic acid for the ICP test. The ICP test results show that the Pd–Co molar ratio is 2.94 : 1, while the Pd–Co molar ratio of the reactant was 5 : 4, which demonstrate that the Pd^{2+} was not adsorbed but doped in the nanocatalyst. Moreover, in the preparation stage, we use EtOH as the reducing agent. Thus, if some Pd^{2+} ions were absorbed, they will be reduced to Pd NPs.

The porous properties of the samples were analyzed by nitrogen sorption analysis. Before measurement, the sample was heated at 60 °C for 10 h under vacuum to dehydrate completely according to the results of thermogravimetric analysis. The BET surface area of $Co_3[Co(CN)_6]_2$ was found to be 459.6 m^2 g^{-1} and that of Pd–$Co_3[Co(CN)_6]_2$was 470.8 m^2 g^{-1}. Due to the contribution of small NPs with 5 nm in size, the BET surface area of Pd–$Co_3[Co(CN)_6]_2$ was slightly larger than $Co_3[Co(CN)_6]_2$. As shown in Fig. 5a and 5b, the adsorption and desorption isotherms of $Co_3[Co(CN)_6]_2$ and Pd–$Co_3[Co(CN)_6]_2$ are also quite similar. The adsorption isotherms display steep nitrogen gas uptake at low relative pressures (P/P_0 < 0.001) reflecting abundant micropore structure, a slight hysteresis loop implying a spot of mesopore and a sharp rise at medium and high pressure regions (P/P_0 = 0.8–1.0) indicating the size of MOF. The pore size distribution of $Co_3[Co\text{-}(CN)_6]_2$ and Pd–$Co_3[Co(CN)_6]_2$ can be obtained from the supplied results by using the sorption apparatus, as shown in Fig. 5c and 5d. The results demonstrate that the narrow porous volume distribution is about 3 nm in pore size, which indicates that the NPs which formed the nanocubes are porous in structure. Additionally, another narrow porous volume distribution is about 0.5 nm, which is consistent with the pore size of the $M^{II}_3[M^{III}(CN)_6]_2$ porous framework structure.[30] Actually, the heterogeneous porous structure is favorable for the catalysis

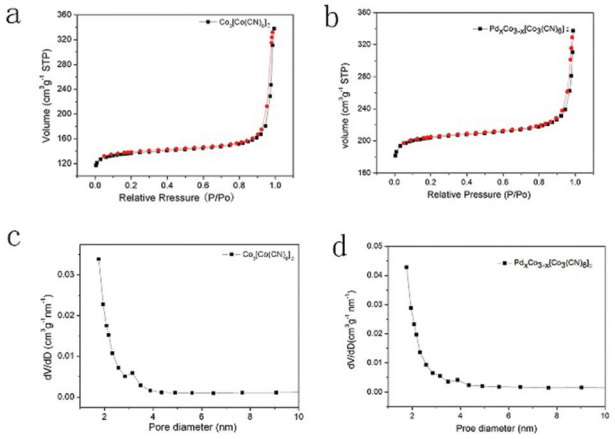

Fig. 5 Nitrogen adsorption (black) and desorption (red) isotherms of: (a) $Co_3[Co(CN)_6]_2$ and, (b) Pd–$Co_3[Co(CN)_6]_2$. Pore size distributions of: (c) $Co_3[Co(CN)_6]_2$ and Pd–$Co_3[Co(CN)_6]_2$.

process. The macroporous structure accelerates the mass transfer of reactants and products, and the micropore of an appropriate size is beneficial for anchoring metal catalysts. It should be noted that the peak at 3 nm in Fig. 5d almost disappeared, which indicated that the 3 nm pore of $Co_3[Co(CN)_6]_2$ was almost covered by Pd NPs.

The possible formation mechanism of hybrid NPs can be inferred from previous results. Firstly, Pd^{2+} ions were absorbed by MOF supports in the cavities and channels. Secondly, Pd^{2+} ions replaced Co^{2+} and became $Pd_3[Co(CN)_6]_2$ due to the lower k_{sp} of $Pd_3[Co(CN)_6]_2$. Finally, the redundant absorbed Pd^{2+} ions were reduced by EtOH to the Pd element, which assembled and nucleated in the cavities and channels of MOF supports.

To evaluate the catalytic ability of the MOF supported Pd NPs, the Suzuki cross-coupling reaction was carried out as a model reaction. The reactions were conducted using ethanol as the solvent and K_2CO_3 as the base. As shown in Table 1, iodobenzene and bromobenzene show good results due to their high reactivity even at room temperature (Table 1, entries 1–3). Then, 4-bromotoluene was used instead of bromobenzene to confirm that the biphenyl was cross coupled by arylhalides and phenylboronic acid rather than by the self-coupling of phenylboronic (Table 1, entry 4). The result shows that the yield of 4-phenyltoluene was up to 99%, with very little biphenyl generated. As for chlorobenzene and 4-chlorotoluene (Table 1, entries 5 and 6), the effect of substituted groups in the substrates was also investigated. Although the tendency shows that the conversion of substituted substrates is lower than the unsubstituted ones, most of the reactions can provide satisfactory yields by increasing the reaction temperature and time (Table 1, entries 7 and 8). For example, as high as 86.2% yield can be obtained by increasing the reaction temperature to 80 °C and time up to 4 h for chlorobenzene reaction. These results determinate our catalyst ability can reach the performance of Pd catalysts with organic phosphine ligands and be

Table 1 Suzuki reactions catalyzed by Pd–$Co_3[Co(CN)_6]_2$ catalysts

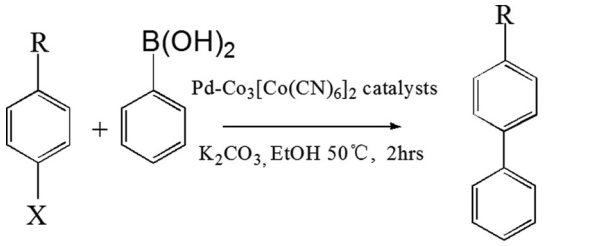

Entry	R	X	Time (h)	Yield[a] (%)	TOF (h^{-1})
1	H	I	2	>99	111
2	H	Br	2	>99	111
3	H	Br	12[b]	>99	9.3
4	CH_3	Br	2	>99	111
5	H	Cl	2	39.4	44
6	CH_3	Cl	2	32.6	36
7	H	Cl	4[c]	86.2	48
8	CH_3	Cl	4[c]	83.1	46
9	NO_2	Cl	4[c]	77.3	43
10	COOH	Cl	4[c]	73.8	42
11	OH	Cl	4[c]	75.4	42
12	NH_2	Cl	4[c]	80.4	44
13	H	I	2[d]	—	—

Reaction conditions: 1 mg of Pd–$Co_3[Co(CN)_6]_2$ catalysts (Pd 47.9 wt%), 1 mmol arylhalide, 1.2 mmol phenylboronic acid, and 3 mmol K_2CO_3, EtOH (30 mL), at 50 °C for 2 h. [a] Isolated yield. [b] At room temperature. [c] At 80 °C. [d] Pure $Co_3[Co(CN)_6]_2$ as the catalyst.

much better than tradition Pd NPs. To investigate the universality of aryl chlorides, substituents of $-NO_2$, –COOH, –OH, $-NH_2$, were employed (Table 1, entries 9–12). These results demonstrate that both aryl chlorides bearing electron-withdrawing groups such as $-NO_2$, –COOH and aryl chlorides bearing electron-donating substituents such as $-CH_3$, –OH, and $-NH_2$ at the *para* position gave the desired products in moderate yields. Also, the mass balance based on the GC results indicated that no side reactions were involved. Pure MOF supports were not able to catalyze the reaction (Table 1, entry 13).

Separation, reusability, stability, and leaching of the catalysts are crucial for practical applications of nanocatalysts. Firstly, the catalysts can be easily separated and recovered by centrifugation due to the MOF supports with size on the nanometre scale. Secondly, this nanocatalyst can be reused eight times with no obvious decrease of conversion rate (Fig. 6a). Moreover, the kinetic studies of four cycles showed that the initial rates and the subsequent rates of each cycle were not reduced even for chlorobenzene reaction at high temperatures (Fig. 6b). Thirdly, this catalyst demonstrated great thermal stability with high activity at elevated temperatures (Table 1, entries 7 and 8). The XRD pattern (Fig. S1a†) and SEM image (Fig. 7a and Fig. S1a†) of the catalyst after the reaction under reflux conditions indicated that phase composition and the surface morphology of the nanocatalysts were not changed. Compared with the previous result, the XPS spectrum (Fig. 7b) of the catalyst after the high temperature reaction shows that no oxidation reaction happened. Lastly, Pd leaching and drop-

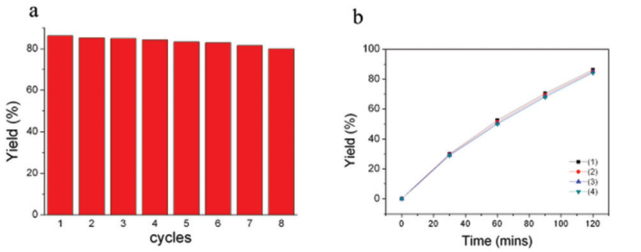

Fig. 6 Catalytic results of the Suzuki reaction of chlorobenzene (reaction conditions similar to Table 1, entry 7). (a) The yield in different cycles. (b) Kinetic profiles for coupling reactions of five cycles.

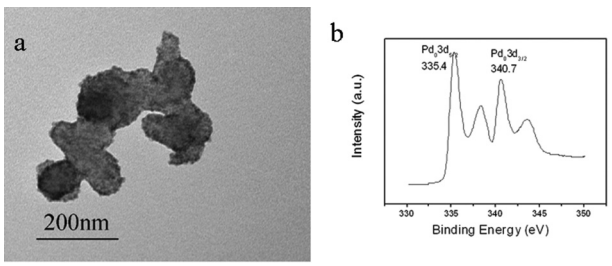

Fig. 7 (a) TEM image of Pd–$Co_3[Co(CN)_6]_2$ catalysts after reaction. (b) XPS spectrum of Pd nanocatalysts after reaction.

ping from the catalysts into the reaction mixture were not observed. The Pd content in the filtrate after the first reaction as well as after five cycles was all found to be lower than 100 ppb by ICP-AES, indicating less Pd loss even after five cycles. Furthermore, the catalysts after eight cycles were analyzed by ICP-AES. The molar ratio of Pd and Co was not changed which indicated that few Pd NPs dropped from MOF supports. The results suggested that the Pd element loss was due to element leaching in the Suzuki reaction rather than dropping of MOF supports.[35]

We compared our results with those of Pd-based catalysts reported in the last year. Taking the reaction of bromobenzene with chlorobenzene as an example; the results are listed in Table S2.† Compared with other Pd based catalysts such as Pd–PPh_3 and Pd–NHC, our catalyst can reach almost the same catalytic efficiency as the reported ones. Our catalyst enjoys several advantages including simple preparation, excellent separation and reusability. On the other hand, our catalysts show much better catalytic performance than the traditional supported Pd(0) NPs in terms of short reaction time and low reaction temperatures.

There are four reasons why our catalyst has high catalytic activity even in the Suzuki coupling of aryl chlorides: (1) the Pd NPs of almost 3 nm are appropriately small and clean without other organic groups; (2) amounts of cavities and channels of the MOF supports benefit reagent adsorption. In traditional catalytic theory, adsorption is the first and important step: (3) the metal nodes of MOF usually have unique catalytic coordination environments. In $Co_3[Co(CN)_6]_2$ NPs, Co^{2+} ions may provide an extra electron to Pd NPs to maintain charge balance. Thus, it is reasonable to expect that the Pd sites with the energetic electrons will exhibit superior catalytic activity to that of pure palladium NPs alone; (4) two valent states Pd including Pd(0) and Pd(II) exist in the catalyst. They may be able to convert easily and in both states Pd can catalyze the Suzuki reaction. Therefore, to understand the synergistic effect of MOF supports and Pd NPs, the performance of different kinds of nanocatalysts' catalytic ability for chlorobenzene reaction was tested (Table S2†). Four types of Pd-based NPs respectively are Pd doped $Co_3[Co(CN)_6]_2$, whose Pd states were Pd(II), $Co_3[Co(CN)_6]_2$@Pd (Fig. S3†), whose Pd states were Pd(0), Pd–$Co_3[Co(CN)_6]_2$, this catalyst, whose Pd states were combined Pd(II) and Pd(II), and Pd–Fe_3O_4@C,whose Pd(0) states were with low surface area supports. From these results, we can confirm that the channels and cavities of MOF, Pd(II) and Pd(0) contributed to the reaction, even when the MOF supports were not able to catalyze the reaction (Table 1, entry 9).

Experimental

Synthesis of MOF nanocrystals

Typical synthetic experiments were as follows: solution A: 0.04 mmol $K_3[Co(CN)_6]_2$ and 0.3 g PVP were dissolved in 10 mL distilled water under agitated stirring to obtain an absolute transparent solution. Solution B: 0.075 mmol of $Co(CH_3COO)_2{\cdot}nH_2O$ was dissolved in 10 mL distilled water. Solution B was added into solution A slowly and regularly using a syringe to form a red colloidal solution. The whole reaction process was carried out at room temperature with agitated stirring. After 10 min, the reaction was aged at room temperature without any interruption for 24 h. The resulting pink precipitation was filtered and washed several times with absolute ethanol and finally dried in an oven at 60 °C.

Synthesis of Pd–$Co_3[Co(CN)_6]_2$ microspheres

0.01 g of $Co_3[Co(CN)_6]_2$ was dissolved in 20 mL water solution. 10 mL palladium chloride water solution (1 g L^{-1}) was slowly added into the above mixture solution at 30 °C in 10 min with vigorous magnetic stirring, followed by the addition of 5 mL EtOH. About four hours later, the solid products were collected by centrifugation and were washed with water several times. The products were dried under vacuum. The solid product was dissolved in concentrated nitric acid and analyzed by using an inductively coupled plasma atomic emission spectrometer (ICP-AES) to determine the content of Pd (47.9 wt%).

Catalytic reaction

For Suzuki cross-coupling reactions, 1 mg of Pd–$Co_3[Co(CN)_6]_2$ catalysts, 1 mmol arylhalide, 1.2 mmol phenylboronic acid, and K_2CO_3 (3 mmol) were added to 30 mL alcohol. The reactions were carried out at 50 °C under reflux conditions for 2 h or at room temperature for 12 h. Then, the catalysts were collected by centrifugation, and the reaction system was analyzed by gas chromatography (GC).

Conclusions

In summary, we demonstrated a simple approach for the large-scale synthesis of Pd–MOF hybrid NPs by a two-step process. The hybrid composite is composed of a large amount of 3 nm-sized Pd nanocrystals with a 100 nm-sized $Co_3[Co(CN)_6]_2$ nanocluster. The formation process of hybrid NPs is *via* adsorption and reduction of noble metallic ions, which can be extended to achieve the synthesis of various noble metal–$Co_3[Co(CN)_6]_2$ hybrid NPs. The nanocrystals exhibited good activities for various Suzuki coupling reactions especially the coupling of aryl chlorides due to their unique structure. Furthermore, the nanocrystals could be easily separated and could be used repeatedly 8 times with minor variation of catalytic activity. The Pd–MOF catalysts have, the advantages of heterogeneous (*e.g.*, low cost, air-stability, easy separation, and good reusability) and homogeneous systems (*e.g.*, high yield) without using toxic chemicals, and have the potential to be used widely in Pd catalyst systems.

Acknowledgements

Thanks for the help of Dr Yang Wang at the Hefei University of Technology in the area of transmission electron microscopy. This work was supported by the National Natural Science Foundation (Grants 21271163 and U1232211). Research supported by the CAS/SAFEA international partnership program for creative research teams. The author Ren Li thanks for the financial support from china scholarship council (CSC, 201500730008).

Notes and references

1 A. Fihri, M. Bouhrara, B. Nekoueishahraki, J. M. Basset and V. Polshettiwar, *Chem. Soc. Rev.*, 2011, **40**, 5181.
2 K. C. Nicolaou, P. G. Bulger and D. Sarlah, *Angew. Chem., Int. Ed.*, 2005, **44**, 4442.
3 G. C. Fortman and S. P. Nolan, *Chem. Soc. Rev.*, 2011, **40**, 5151.
4 J.-P. Corbet and G. Mignani, *Chem. Rev.*, 2006, **106**, 2651–2710.
5 A. Zapf, A. Ehrentraut and M. Beller, *Angew. Chem., Int. Ed.*, 2000, **39**, 4153.
6 E. A. B. Kantchev, C. J. O'Brien and M. G. Organ, *Angew. Chem., Int. Ed.*, 2007, **46**, 2768.
7 L. Botella and C. Nájera, *Angew. Chem., Int. Ed.*, 2002, **41**, 179.
8 G. Borja, A. Monge-Marcet, R. Pleixats, T. Parella, X. Cattoën and M. Wong Chi Man, *Eur. J. Org. Chem.*, 2012, 3625.
9 R. Akiyama and S. Kobayashi, *J. Am. Chem. Soc.*, 2003, **125**, 3412.
10 A. Balanta, C. Godard and C. Claver, *Chem. Soc. Rev.*, 2011, **40**, 4973.
11 N. B. McKeown and P. M. Budd, *Chem. Soc. Rev.*, 2006, **35**, 675.
12 H. Furukawa and O. M. Yaghi, *J. Am. Chem. Soc.*, 2009, **131**, 8875.
13 D. Dang, P. Wu, C. He, Z. Xie and C. Duan, *J. Am. Chem. Soc.*, 2010, **132**, 14321.
14 G. Férey, C. Mellot-Draznieks, C. Serre, F. Millange, J. Dutour, S. Surblé and I. Margiolaki, *Science*, 2005, **309**, 2040.
15 T. Tozawa, J. T. Jones, S. I. Swamy, S. Jiang, D. J. Adams, S. Shakespeare, R. Clowes, D. Bradshaw, T. Hasell and S. Y. Chong, *Nat. Mater.*, 2009, **8**, 973.
16 C. D. Wood, B. Tan, A. Trewin, F. Su, M. J. Rosseinsky, D. Bradshaw, Y. Sun, L. Zhou and A. I. Cooper, *Adv. Mater.*, 2008, **20**, 1916.
17 H. Furukawa, N. Ko, Y. B. Go, N. Aratani, S. B. Choi, E. Choi, A. Ö. Yazaydin, R. Q. Snurr, M. O'Keeffe and J. Kim, *Science*, 2010, **329**, 424.
18 Z. Y. Gu and X. P. Yan, *Angew. Chem., Int. Ed.*, 2010, **49**, 1477.
19 J. Lee, O. K. Farha, J. Roberts, K. A. Scheidt, S. T. Nguyen and J. T. Hupp, *Chem. Soc. Rev.*, 2009, **38**, 1450.
20 A. Corma, H. Garcia and F. Llabrés i Xamena, *Chem. Rev.*, 2010, **110**, 4606.
21 H. R. Moon, D.-W. Lim and M. P. Suh, *Chem. Soc. Rev.*, 2013, **42**, 1807.
22 W. Xuan, C. Zhu, Y. Liu and Y. Cui, *Chem. Soc. Rev.*, 2012, **41**, 1677.
23 K. K. Tanabe and S. M. Cohen, *Chem. Soc. Rev.*, 2011, **40**, 498.
24 M. Zhao and C. D. Wu, *Acc. Chem. Res.*, 2014, **47**, 1199.
25 Y. K. Hwang, D. Y. Hong, J. S. Chang, S. H. Jhung, Y. K. Seo, J. Kim, A. Vimont, M. Daturi, C. Serre and G. Férey, *Angew. Chem., Int. Ed.*, 2008, **47**, 4144.
26 S.-i. Ohkoshi, Y. Abe, A. Fujishima and K. Hashimoto, *Phys. Rev. Lett.*, 1999, **82**, 1285.
27 S. S. Kaye and J. R. Long, *J. Am. Chem. Soc.*, 2005, **127**, 6506.
28 S. Ferlay, T. Mallah, R. Ouahes, P. Veillet and M. Verdaguer, *Nature*, 1995, **378**, 701.
29 J. G. Moore, E. J. Lochner, C. Ramsey, N. S. Dalal and A. Stiegman, *Angew. Chem., Int. Ed.*, 2003, **42**, 2741–2743.
30 L. Hu, P. Zhang, Q.-w. Chen, N. Yan and J.-y. Mei, *Dalton Trans.*, 2011, **40**, 5557.
31 L. Hu, P. Zhang, Q.-w. Chen, J.-y. Mei and N. Yan, *RSC Adv.*, 2011, **1**, 1574.
32 L. Hu, J.-y. Mei, Q.-w. Chen, P. Zhang and N. Yan, *Nanoscale*, 2011, **3**, 4270.
33 L. Hu, Y. Huang and Q. Chen, *J. Alloys Compd.*, 2013, **559**, 57.
34 G. Kumar, J. R. Blackburn, R. G. Albridge, W. E. Moddeman and M. M. Jones, *Inorg. Chem.*, 1972, **11**, 296.
35 Z. Q. Niu, Q. Peng, Z. B. Zhuang, W. He and Y. D. Li, *Chem. – Eur. J.*, 2012, **18**, 9813–9817.

